



# Boosting of the Optical Properties, and Electrical Conductivity of Polymethyl Methacrylate (PMMA)/ Polystyrene (PS) Blend with Zinc Oxide Nanoparticles for High-Performance Energy Storage Devices

Ghadah Abdulrahman AlZaidy<sup>1</sup>

Received: 22 April 2024 / Accepted: 17 May 2024

© The Author(s), under exclusive licence to Springer Science+Business Media, LLC, part of Springer Nature 2024

## Abstract

Nanocomposite films were fabricated by employing a solution casting technique, incorporating varying weight percentages of ZnO NPs into a PMMA/PS blend. Through analyses via X-ray diffraction (XRD) and transmission electron microscopy (TEM), it was evident that the hexagonally shaped ZnO NPs possessed high purity, falling within the size range of 25 to 45 nm. Both XRD and FT-IR investigations highlighted a decrease in the semicrystalline character of the PMMA/PS blend with the incorporation of ZnO NPs, attributed to interactions between the functional groups of the host matrix and the nanofillers. Moreover, UV/visible spectra revealed a reduction in the optical bandgap energies of the nanocomposites as the ZnO NP content increased, with direct energy gap values decreasing from 4.45 eV to 3.12 eV, and indirect energy gap values decreasing from 3.33 eV to 1.82 eV. Dielectric properties, electrical conductivity, and impedance of the samples were investigated over a frequency range of 0.1–10<sup>6</sup> Hz. Notably, enhancements in dielectric permittivity, dielectric loss, and AC conductivity were observed with increasing concentrations of ZnO NPs. The advantageous nanodielectric characteristics of these hybrid samples were evident, particularly in their low permittivity at high frequencies. Additionally, analysis utilizing impedance components  $Z'$  and  $Z''$  facilitated the creation of an equivalent electrical circuit. Overall, PMMA/PS-ZnO nanocomposites exhibit promising potential in the realm of flexible optoelectronic and energy storage devices, owing to their adjustable optical energy gap, frequency-dependent AC conductivity, and versatile composition-dependent permittivity.

**Keywords** PMMA/PS · ZnO NPs · Optical parameters · AC conductivity · Energy storage

## 1 Introduction

The development of polymer nanocomposites has garnered considerable attention from both scientists and industrial researchers over the past two decades [1]. This surge in interest is not solely attributed to their amalgamation of advantageous properties like low weight, cost-effectiveness, and straightforward synthesis [2]. More prominently, it arises from their intrinsic versatility and multifaceted capabilities. These attributes make polymer nanocomposites well-suited for a broad spectrum of applications in optoelectronic

technology, including the development of display devices and solar cells [3, 4]. Polymer nanocomposites entail the incorporation of nanoparticles into a polymer or copolymer matrix. The synergistic combination of unique properties from polymers and nanoparticles within these engineered composites has the potential to generate materials of significant interest, with applications in both fundamental research and technological advancements.

Polymethyl methacrylate (PMMA) is a transparent polymer known for its distinctive characteristics, encompassing lightweight, high light transmittance, chemical resistance, and resilience to corrosion and weathering. Despite these merits, PMMA faces constraints in the optoelectronic sector, including applications in compact discs (CDs) and optical fiber manufacturing. This limitation arises from its relatively low glass transition temperature, approximately 100.8 °C, which hinders its usage as an inner glazing

✉ Ghadah Abdulrahman AlZaidy  
gazaidy@uqu.edu.sa

<sup>1</sup> Department of Physics, College of Science, Umm Alqura University, Makkah, Saudi Arabia

material and can result in distortion [5]. Hence, the cost-effective enhancement of PMMA's physical attributes often involves blending it with other compatible polymers. In this regard, polystyrene (PS) emerges as a highly effective industrial material employed in various domestic applications, including optical lenses and laser-active mediums, owing to its commendable optical properties [6]. Furthermore, the enhancement of polymeric blends can be significantly achieved by introducing varying wt% of nanofillers, thereby altering their optical and electrical properties [7]. Furthermore, its biocompatibility, along with notable photocatalytic activity, mechanical properties, and thermal stability, positions ZnO as an excellent candidate for various applications. These exceptional characteristics render it suitable for deployment in photodetectors, gas sensors, solar cells, and photocatalysis.

Numerous researchers have highlighted the versatile applications of low-cost PMMA/PS polymeric blends filled with different metal oxide nanoparticles [8]. El-Morsy, M. A., et al. [9] observed that the morphological, optical properties and electrical conductivity of the PMMA-PS polymer blend were improved through the incorporation of silver nanoparticles. V. Khrenov has explored the creation of polymer/ZnO nanocomposites, including the discussion of PMMA/ZnO composites [10]. Kadhim and Ehsan [11] investigated novel PMMA-PVA/graphene oxide (GO) nanocomposites. Their work demonstrates a successful method for fabricating these nanocomposites with tunable GO content. These findings suggest potential applications in radiation shielding, optoelectronic devices, and ultraviolet filters. Kadim, et al. [12] investigated the effect of incorporating corn starch nanoparticles (CSNPs) into a PVA/PMMA/PAAm (PPP) blend. They found that CSNPs improved the optical properties of the nanocomposite films, reducing the bandgap energy and enhancing light absorption. Abdali, Karar [13], developed a novel PEO/Al@SiO<sub>2</sub> core-shell polymer nanocomposite film for stretchable devices. The nanocomposite exhibited improved optical properties with a reduced bandgap and enhanced dielectric properties compared to the PEO polymer alone. These findings suggest its potential application in the fabrication of flexible optoelectronic devices. G. Soni et al. conducted a study on the optical, mechanical, and structural properties of thin films composed of PMMA and SiO<sub>2</sub>. The findings indicated that an increment in the wt% of SiO<sub>2</sub> nanoparticles caused in a narrowing of the optical bandgap [14]. Al-Bataineh, Qais M., et al. [15], investigated the influence of ZnO, CuO, TiO<sub>2</sub>, and SiO nanoparticles on the optical parameters of pure PMMA. Cinausero, Nicolas, et al. [16], endeavored to improve the thermal properties of PMMA-PS nanocomposite through the incorporation of alumina oxides. Wie, Jaehyun, and Jooheon Kim [17] introduced a method

aimed at improving thermal conductivity through the utilization of PMMA-PS composite, coupled with the addition of multi-walled carbon nanotubes (MWCNT). Alsharaeh, Edreese H [18], documented a substantial enhancement in the electrical properties of PMMA, PS, and PMMA/PS copolymer upon the incorporation of silver nanoparticles (Ag NPs). Sahal Saad Ali [19] endeavored to enhance the electrical conductivity of PMMA-PS through the incorporation of multi-walled carbon nanotubes (MWCNT), aiming for optimization. Mathur, R. B., et al. [20], investigated the mechanical properties and electrical conductivity of composites comprising multiwalled carbon nanotubes boosted PS-PMMA. Rashid, Farhan Lafta, et al. [21], demonstrated that the absorption coefficient, extinction coefficient, refractive index, as well as the dielectric loss and dielectric constants of the PS-PMMA co-polymer, exhibit an increase corresponding to the rise in sodium fluoride concentration.

While numerous studies have explored the influence of various organic and inorganic additives on the morphological, optical parameters, and electrical conductivity of PS/PMMA composites [7–16], limited attention has been given to the doping impact of ZnO on the characteristics of PMMA/PS polymer blend. This study aims to improve the morphological, optical features, and electrical conductivity of the PMMA/PS blend through the incorporation of ZnO nanoparticles. The samples were characterized via XRD, FT-IR, UV/Vis., and AC conductivity techniques. A novel aspect of this research lies in the one-step creation of PMMA/PS samples, employing high-purity ZnO nanoparticles. ZnO NPs were selected as dopants due to their ease of preparation, repeatability, low cost, and consistency.

To objectively assess the novelty of this study, an extensive literature review was conducted to identify similar research endeavors focusing on the applications of PMMA-PS-ZnO nanocomposite or comparable approaches in optoelectronic devices. Limited studies have employed PMMA in conjunction with PS for thin film fabrication. Structural analysis and chemical characterization of the samples were conducted by X-ray diffraction and FTIR. The shapes and sizes of the zinc oxide nanoparticles were investigated through transmission electron microscopy (TEM). Additionally, the optical and electrical properties of the prepared films were assessed through UV-vis spectrophotometry and AC conductivity measurements.

## 2 Experimental Work

### 2.1 Chemicals

For this study, commercially available analytical-grade materials and solvents were employed. Polystyrene

( $M_w = 100 \text{ kg mol}^{-1}$  with a purity of 98%.) and polymethyl methacrylate ( $M_w = 30 \text{ kg mol}^{-1}$  with a purity of 99%.) were obtained from BDH Co. Zinc oxide nanoparticles (ZnO) with a purity of 98.997% and a particle size of 34.2 nm were purchased from Sigma Aldrich, Germany. Deionized water, Sodium hydroxide, ethanol, and chloroform, all analytical grade, were also obtained from Sigma Aldrich, Germany. Every solution was meticulously prepared using deionized water, and chloroform.

## 2.2 Synthesis of ZnO NPs

To synthesize ZnO NPs, a standard procedure was followed. A 0.5 M aqueous solution of zinc nitrate ( $\text{Zn}(\text{NO}_3)_2 \cdot 4 \text{H}_2\text{O}$ ) and a 0.8 M aqueous solution of sodium hydroxide (NaOH) were prepared using deionized water. The NaOH solution was heated to approximately 50 °C, and then the  $\text{Zn}(\text{NO}_3)_2$  solutions were added dropwise over 30 min to the heated solution with vigorous stirring. The sealed beaker was maintained under these conditions for 1 h. The resulting ZnO nanoparticles were washed with deionized water and ethanol, followed by drying in ambient air at around 70 °C. The purity of the ZnO material achieved was high. The purification process ensured that the synthesized nanoparticles were of high quality (approximately 96%), with minimal impurities present. Transmission electron microscopy was used for imaging the synthesized ZnO nanoparticles.

## 2.3 Synthesis of PMMA&PS/ZnO Nanocomposites

The experimental procedure involved dissolving specific amounts (0.5 g each) of PMMA and PS in separate glass bottles containing 25 mL of chloroform for each polymer. Magnetic stirring at 45 °C for 1 h ensured a homogeneous PMMA/PS blend in a 50/50 wt% ratio. Meanwhile, the mandatory quantity of ZnO (0.064 g) was dispersed in 20 mL of distilled water under magnetic stirring. This ZnO suspension underwent sonication for 15 min at 20 kHz and 500 W using a high power probe sonicator (model UIP-500hdT, USA). After sonication, the ZnO was incorporated into PMMA/PS composite based on calculations following established principles [22]:

**Table 1** Weight ratios of PMMA&PS and ZnO nanoparticles

| Samples         | PMMA&PS (g) | ZnO (g) | Total |
|-----------------|-------------|---------|-------|
| PMMA            | 0.5         | -       | -     |
| PS              | 0.5         | -       | -     |
| Pure PMMA/PS    | 1.0         | -       | -     |
| PMMA/PS -1% ZnO | 0.996       | 0.004   | 1     |
| PMMA/PS -3% ZnO | 0.988       | 0.012   | 1     |
| PMMA/PS -5% ZnO | 0.980       | 0.020   | 1     |
| PMMA/PS -7% ZnO | 0.972       | 0.028   | 1     |

$$Wt\% = \frac{W_f}{W_b + W_f} \quad (1)$$

Here  $w_b$  and  $w_f$  denote the weight of the polymers and metal oxide, respectively. Details of the weight ratios used can be found in Table 1. The solution was continuously stirred at 50 °C for 30 min for uniform dispersion. To further enhance nanoparticle homogeneity, the PMMA/PS-ZnO solution underwent a 15-minute probe sonication treatment. The resulting solution was then cast onto Petri dishes and oven-dried at 45 °C for 2 days. This process yielded free-standing PMMA/PS-ZnO films with thicknesses ranging from 0.07 to 0.09 mm.

## 2.4 Characterizations

**a-X-ray Diffraction (XRD)** A PANalytical X'Pert PRO system operating at 30 kV with Cu K $\alpha$  radiation was used for XRD analysis. The samples were scanned across a  $2\theta$  range of 5–70°. This technique aimed to identify any changes in the crystal structure of the composite caused by the incorporation of ZnO nanoparticles.

**b-Transmission Electron Microscopy (TEM)** A JEOL JSM-100 CX instrument was employed for TEM analysis to investigate the morphology, particularly the shape and size distribution, of the ZnO nanoparticles within the polymer blend.

**c-Fourier-Transform Infrared (FT-IR) Spectroscopy** Functional groups present in the composites were characterized using a Nicolet iS10 spectrometer (Thermo Fisher Scientific, USA) in the mid-infrared range (4000–400  $\text{cm}^{-1}$ ). This technique helps identify potential interactions between the polymer blend and the ZnO nanoparticles.

**d-UV-Visible (UV-Vis) Spectroscopy** The optical properties of the films were analyzed using a JASCO V-570 instrument (JASCO Corporation, Japan) across a wavelength range of 190–1100 nm. This technique provides information about light absorption and potential bandgap changes due to the presence of ZnO.

**e-Impedance Spectroscopy** Electrical conductivity and related phenomena were investigated using impedance spectroscopy at room temperature. A computer-controlled phase-sensitive multimeter (PSM-1700) was employed

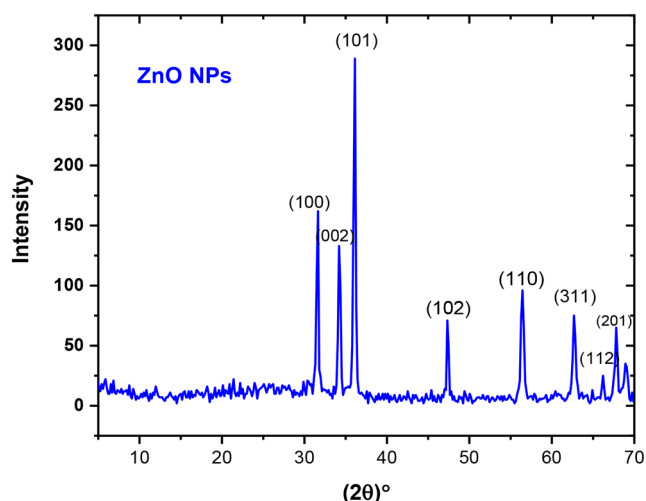


**Fig. 1** XRD patterns of zinc oxide nanoparticles

within a frequency range of 0.1 Hz to 1 MHz. This technique helps understand the electrical behavior of the composites.

### 3 Results and Discussion

#### 3.1 XRD Spectra

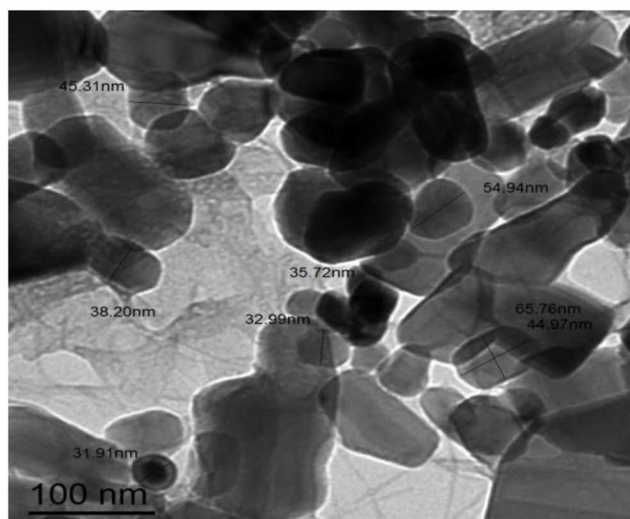
**Fig. 1** illustrates the XRD spectra of ZnO NPs. The observed peaks at  $2\theta = 31.57^\circ$ ,  $34.21^\circ$ ,  $36.24^\circ$ ,  $47.45^\circ$ ,  $56.41^\circ$ ,  $62.59^\circ$ ,  $67.88^\circ$ , and  $69.02^\circ$  correspond to the Miller indices of (100), (002), (101), (102), (110), (311), (112), and (201), respectively. The diffraction peaks of the zinc oxide nanoparticles align closely with JCPDS, card No. 89–0510. This pattern is

indicative of the hexagonal wurtzite crystal structure of ZnO nanoparticles [23]. The crystallite size ( $R$ ) was determined by utilizing the corresponding Full Width at Half Maximum (FWHM) values [24, 25]:

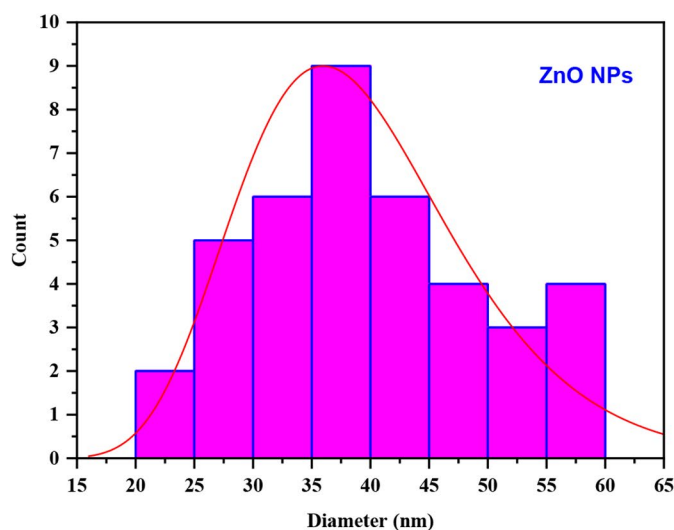
$$R = \frac{L\lambda}{\delta \cos\theta} \quad (2)$$

Here,  $L$  represents the Scherrer constant ( $L = 0.93$ ),  $\lambda$  denotes the wavelength,  $\theta$  is the Bragg angle, and  $\delta$  is the Full Width at Half Maximum (FWHM) of the diffracted halo peak. The ZnO nanoparticles exhibit a size distribution ranging from around 25.5 to nearly 40.15 nm [26]. **Fig. 2** displays the TEM image of ZnO NPs along with the corresponding histogram distribution map. In these visualizations, the ZnO NPs exhibit a crystalline structure, appearing almost hexagonal and irregularly distributed, with crystal diameters ranging between 25 and 45 nm. This observation aligns with the XRD data.

XRD study was used to investigate the formation of the PMMA/PS blend and explore the impact of varying ZnO nanoparticle contents on the blend formation. The XRD patterns for the PMMA/PS-ZnO nanocomposite samples are presented in **Fig. 3**. Notably, **Fig. 3** reveals a broad peak centered at  $2\theta = 19.37^\circ$ , indicating the semicrystalline nature of the host matrix, which comprises both crystalline and amorphous zones. The amorphous broadband decreases in all cases except for the concentration of 3%, which can be attributed to the disturbance of the PMMA/PS polycrystalline structure caused by the introduction of ZnO nanoparticles, as suggested by Rajeh et al. [27]. As noted by Rajeh



(a)



(b)

**Fig. 2** (a) TEM image and (b) histogram of zinc oxide nanoparticles

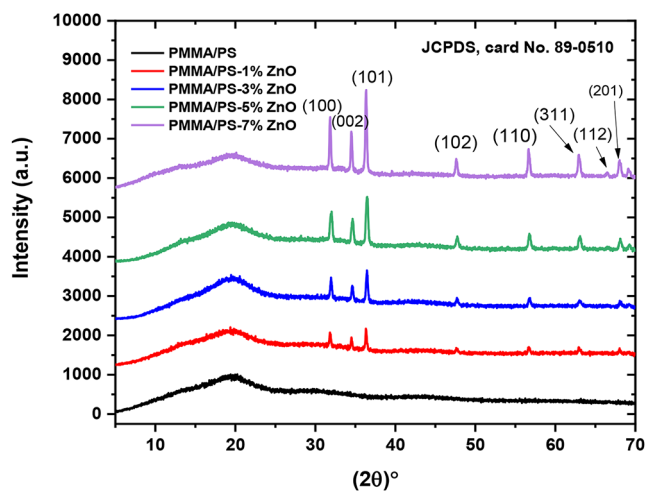


**Fig. 3** XRD patterns of PMMA/PS doped with various wt % of zinc oxide nanoparticles

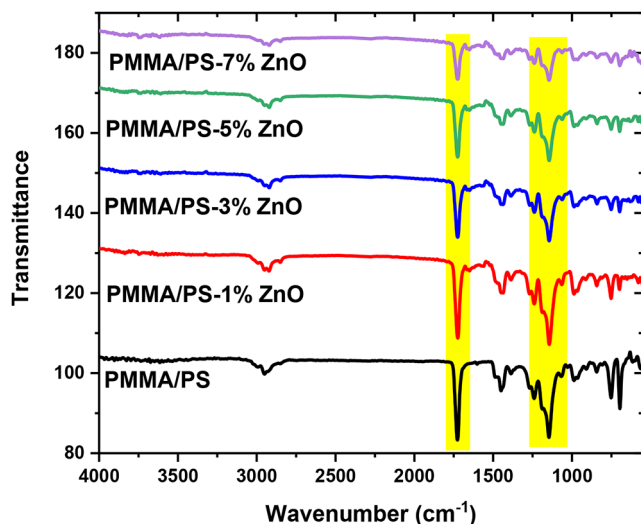


**Fig. 4** FT-IR spectra of PMMA/PS filled with various quantities of zinc oxide nanoparticles

et al., the incorporation of nanofillers leads to a decrease in peak intensity owing to their inherent amorphous nature. This amorphous character plays a role in improving ionic diffusivity and achieving high ionic conductivity, particularly notable in the flexible backbone of amorphous polymers. However, new distinct peaks were identified in the doped PEMA/PMMA at  $2\theta = 31.57^\circ, 34.21^\circ, 36.24^\circ, 47.45^\circ, 56.41^\circ, 62.59^\circ, 67.88^\circ, \text{ and } 69.02^\circ$ . These peaks closely resemble the characteristic XRD peaks of ZnO NPs. This alignment is credited to the interaction between zinc oxide and the polymeric chain, primarily involving the functional group C=O in the polymer blend, as indicated by the FT-IR spectra. Moreover, the crystallinity experiences an increase with the dopant, particularly at a concentration of 3%, owing to the formation of complexes that enhance local ordering in the polymer blend. In this context, zinc

oxide occupies interstitial sites between amorphous phases and establishes connections through H bonds [28].

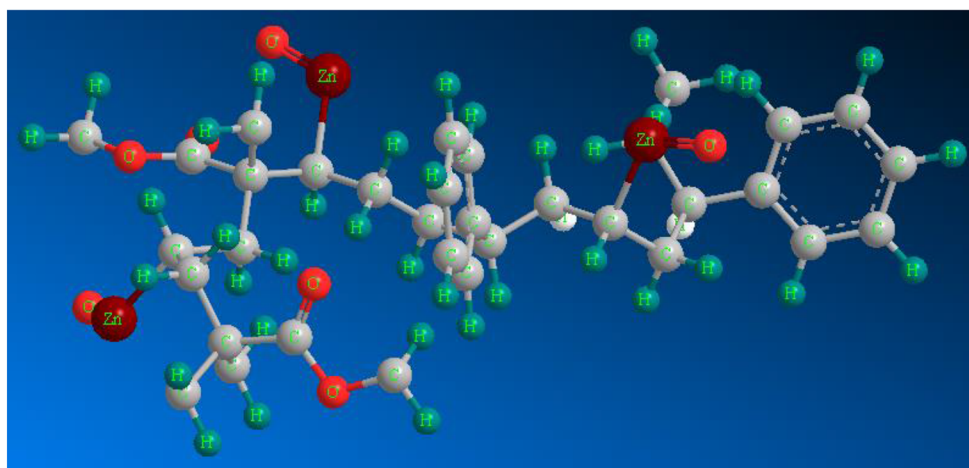
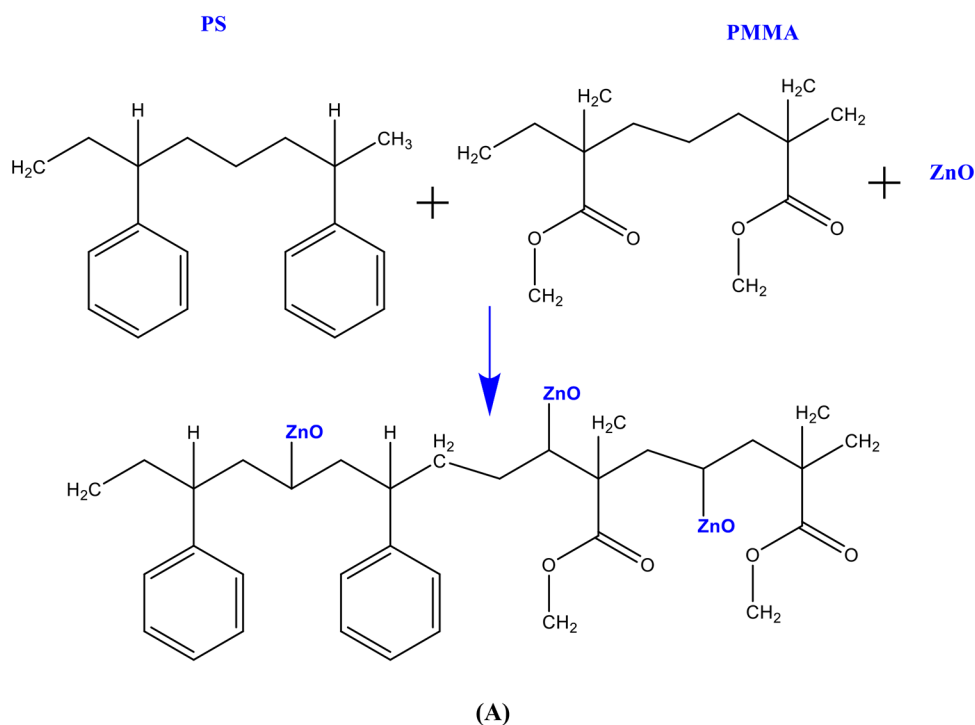
### 3.2 FTIR Analysis

FTIR spectroscopy serves as a valuable method for characterizing intermolecular interaction between groups within self-polymer or different polymeric molecules in the polymer blend. Interactions like as dipole-dipole and hydrogen bonding interactions can cause changes in the absorbance of functional groups or variations in frequency [29]. Fig. 4 presents the FT-IR spectra of virgin PMMA/PS doped with various wt% of ZnO in the range of  $4000\text{--}400\text{ cm}^{-1}$ . The methyl groups' asymmetric and symmetric C–H stretching is responsible for the bands seen at  $2957\text{ cm}^{-1}$  and  $2911\text{ cm}^{-1}$ , respectively. Also, the vibrational band corresponding to C=O stretching is located at around  $1726\text{ cm}^{-1}$ . In polymeric matrices, this double bond serves as a source of charged structural defects known as bipolarons and/or polarons [30]. The asymmetric O–C<sub>2</sub>H<sub>5</sub> bending ( $\gamma(\text{OC}_2\text{H}_5)$ ) and CH<sub>2</sub> twisting (CH<sub>2</sub>) are responsible for the bands seen at  $1445\text{ cm}^{-1}$  and  $1389\text{ cm}^{-1}$ . The absorption band at approximately  $1238\text{ cm}^{-1}$  is assigned to C–O–C stretching vibration. The absorption band at  $1137\text{ cm}^{-1}$  corresponds to the CH<sub>2</sub> scissoring ( $\delta(\text{CH}_2)$ ). The bands at  $983\text{ cm}^{-1}, 843\text{ cm}^{-1}, 756\text{ cm}^{-1}, \text{ and } 696\text{ cm}^{-1}$  are associated with the aromatic C–H deformation vibrations [31]. Additionally, a noticeable trend is observed in the bands within the range of  $1000\text{ cm}^{-1}$  to  $500\text{ cm}^{-1}$ , where their intensity decreases with increasing concentration. These bands are linked to skeletal stretching, coupled with C–H deformation (at  $1000\text{ cm}^{-1}$ ), and are influenced by intermolecular interaction [32]. As the concentration of ZnO increases, there is an obvious reduction in the stretching frequency of C=O (at  $1726\text{ cm}^{-1}$ ) and several other bands. This implies that the observed alterations in the FTIR spectra may be owing to the interactions between ZnO and specific functional groups within the PMMA/PS matrix, potentially involving hydrogen bonding [33]. Scheme 1 depicts the possible interactions between the PMMA, PS, and the zinc oxide.

### 3.3 Optical Properties

The absorption spectra of virgin and doped PMMA/PS samples with ZnO are shown in Fig. 5. The spectra were obtained using a UV-Vis spectrometer at room temperature. The absorption edge can be used to compute the samples' band gaps, which offers important information on the band structure in both crystalline and noncrystalline states. All filled films showed a little increase in absorbance when compared with unfilled samples (Fig. 5), which might be explained by electronic transitions from the bonding molecular orbit.

**Scheme. 1** Possible interaction between the PMMA, PS, and ZnO nanocomposite (A) 2D and (B) 3D



Significantly, the spectra show peaks at 219 and 267 nm, which are linked to electronic transitions from the carbonyl (C=O) groups of the PMMA chain's monomers [34]. Furthermore, the observed phenomena can be attributed to the UV optical absorption bands, which are commonly linked to charge transfer (CT) bands in noncrystalline materials. Remarkably, films made from PMMA/PS-ZnO nanocomposite doped with broadband gap zinc oxide have substantially similar increased absorbance for UV radiations [35]. Moreover, Fig. 4 illustrates that with an increase in zinc oxide quantity in the PMMA/PS nanocomposite samples,

there is a slight red shift observed in the UV absorbance band. The formation of intra- or intermolecular hydrogen bonds (-H) between zinc ions and the nearby functional groups in the PMMA/PS blend is indicated by the change in the absorption band. Following Beer's law, an increase in ZnO concentration is expected to amplify UV absorbance and promote intra- and inter-hydrogen bonding. The phase transition caused by ZnO loading from crystalline to amorphous is theorized to be the cause of the observed shift in the absorption edge of the different ZnO-doped PMMA/PS

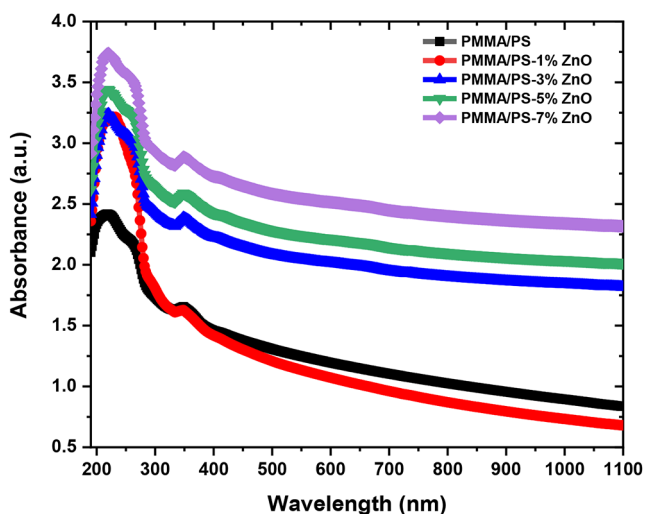


**Fig. 5** UV-Vis spectra of PMMA/PS blend and PMMA/PS doped with various quantities of zinc oxide nanoparticles

polymer blends. This phase change might be reflected in the energy band gap [36].

The values of the energy gap ( $E_g$ ) for both virgin PMMA/PS and PMMA/PS-ZnO nanocomposite samples were determined using the Tauc equation. The high absorption area close to these films' absorption edge was used in this calculation [37, 38]:

$$(\alpha h\nu) = C(h\nu - E_g)^r \quad (3)$$

The calculation of  $E_g$  values involves plotting the  $(\alpha h\nu)^2$  and  $(\alpha h\nu)^{1/2}$  against the energy of the incident photons ( $h\nu$ ). The relationship between  $(\alpha h\nu)^2$  and  $(\alpha h\nu)^{1/2}$  for PMMA/PS-ZnO nanocomposite samples is revealed in Fig. 6 (a, b) as a function of photon energy ( $h\nu$ ). The energy gap ( $E_g$ ) of unfilled PMMA/PS is 4.65 eV. Table 2 provides the  $E_g$  values for PMMA/PS with the addition of 1, 3, 5, and 7 wt% of ZnO NPs. The  $E_g$  values of PMMA/PS decreased from 4.45 to 3.12 eV (Direct) and 3.33 to 1.82 eV (Indirect) as the concentration of ZnO increased. This reduction in  $E_g$  values for PMMA/PS is ascribed to the interaction between metal oxide and the host polymers, leading to the generation of

**Fig. 6** Variations of (a)  $(\alpha h\nu)^2$  and (b)  $(\alpha h\nu)^{1/2}$  with  $h\nu$  of PMMA/PS blend with different content of zinc oxide nanoparticles

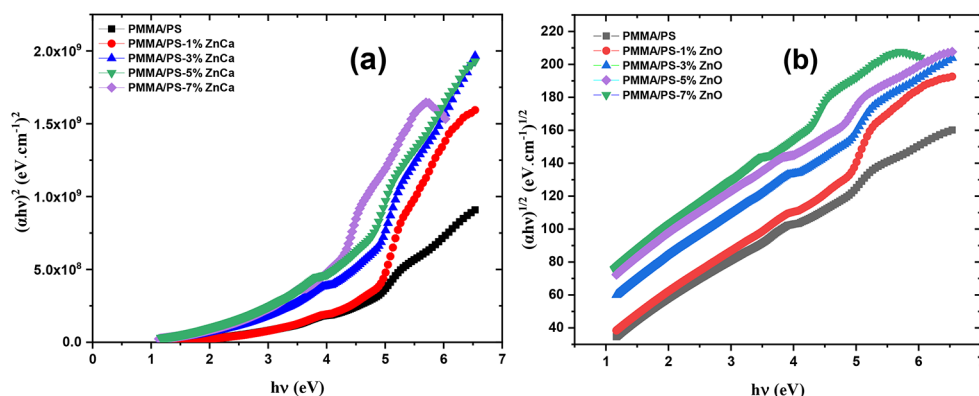


**Table 2** Values of energy bandgap ( $E_g^{Ind.}$  and  $E_g^{Dir.}$  for ZnO and PMMA&PS with different ZnO wt%

| Sample             | $E_g^{Dir.}$ (eV) | $E_g^{Ind.}$ (eV) |
|--------------------|-------------------|-------------------|
| ZnO NPs            | -                 | 3.37              |
| PMMA/PS            | 4.45              | 3.33              |
| PMMA&PS- 1%ZnO NPs | 4.30              | 3.71              |
| PMMA&PS- 3%ZnO NPs | 4.01              | 2.64              |
| PMMA&PS- 5%ZnO NPs | 3.81              | 2.28              |
| PMMA&PS- 7%ZnO NPs | 3.12              | 1.82              |

unstructured defects and micro strains [39]. The density of localized states inside the band gap increases as a result of the formation of unstructured defects and micro strains [40].

### 3.4 Conductivity Analysis

Polymers commonly exhibit frequency-dependent conductivity, a phenomenon associated with a substantial enhancement in the mobility of charge carriers inside the polymer blend [41]. The frequency dependence exhibited by most polymers can be utilized for various applications. Furthermore, it may be applied to enhance complex nanocomposites' electrical characteristics. By employing impedance spectroscopy, the  $\sigma_{ac}$  of the prepared nanocomposite can be calculated using the following equation:

$$\sigma_{ac} = 2f\epsilon'\epsilon_0 \tan \quad (4)$$

Here,  $\tan\delta$  is the dissipation factor,  $f$  denotes the applied frequency, while  $\epsilon_f$  and  $\epsilon_o$  stand for the dielectric constant and free space, respectively. At ambient temperatures, Fig. 7 illustrates the frequency-dependent behavior of PMMA/PS doped with varying wt% of ZnO NPs. The figure demonstrates a consistent increase in conductivity with the rise in ZnO nanoparticle content, indicating that dispersed ZnO nanoparticles contribute to an augmentation in the number of conductive paths. The conductivity of this nanocomposite is thought to rely on various factors, including the type, shape, size, and distribution of the nanofiller within the composite [42]. The increased conductivity likely stems

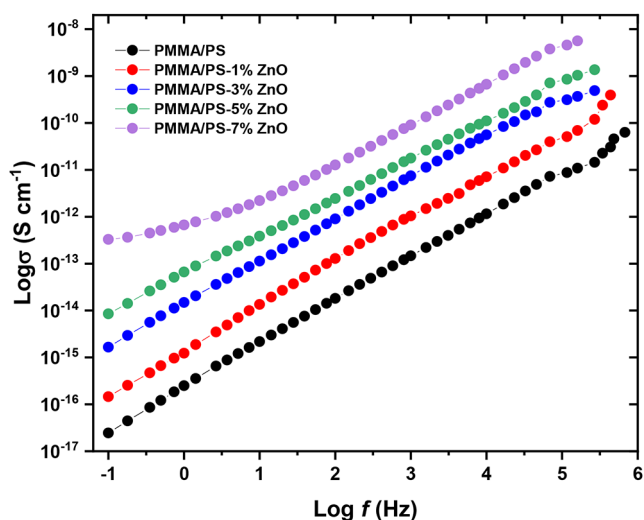


**Fig. 7** The relation between  $\log(\sigma_{ac})$  and  $\log(f)$  for PMMA/PS matrix doped with various quantities of ZnO nanoparticles

**Table 3** The values of  $S$ ,  $\sigma_{dc}$ , and fitting parameters ( $R_b$ ,  $Q_1$ , and  $n_1$ ) of the equivalent circuit for the samples under investigation

| Sample            | $\sigma_{dc}$ (S/cm)   | $S$  | Fitting parameters |                       |       |
|-------------------|------------------------|------|--------------------|-----------------------|-------|
|                   |                        |      | $R_b$ ( $\Omega$ ) | $Q_1$ (F)             | $n_1$ |
| PMMA/PS           | $1.63 \times 10^{-17}$ | 0.69 | $2.23 \times 10^6$ | $4.22 \times 10^{-7}$ | 0.73  |
| PMMA&PS-1%ZnO NPs | $1.15 \times 10^{-16}$ | 0.67 | $8.64 \times 10^5$ | $5.46 \times 10^{-7}$ | 0.65  |
| PMMA&PS-3%ZnO NPs | $1.23 \times 10^{-15}$ | 0.63 | $6.69 \times 10^5$ | $6.35 \times 10^{-7}$ | 0.61  |
| PMMA&PS-5%ZnO NPs | $6.48 \times 10^{-15}$ | 0.58 | $6.55 \times 10^5$ | $7.33 \times 10^{-7}$ | 0.58  |
| PMMA&PS-7%ZnO NPs | $3.14 \times 10^{-13}$ | 0.54 | $5.64 \times 10^5$ | $8.85 \times 10^{-7}$ | 0.51  |

from a combination of additional charge carriers introduced by ZnO nanoparticles and a potential enhancement in the amorphous character of the matrix. This, in turn, lowers the energy barrier, facilitating ion movement [43].

The data in the Fig. 7 reveals a positive correlation between frequency and electrical conductivity for all prepared films. The conductivity of the samples tends to be frequency-dependent, particularly at high frequency, and conforms to the power-law equation proposed by Jonscher [44]:

$$\sigma_{ac}(\omega) = \sigma + A\omega^S \quad (5)$$

Here,  $\sigma_{dc}$  denotes the dc conductivity (specifically, at  $\omega$  equal to zero),  $A$  is a frequency-dependent factor, and  $S$  is an exponent that exhibits variation with frequency. The observations in Table 3 are consistent with the correlated barrier hopping (CBH) model for electrical conduction within the films. This conclusion is based on the observation that all “ $S$ ” values are less than 1 [45, 46]. Moreover, the  $\sigma_{dc}$  values for PMMA/PS-ZnO films exhibit an increase

of approximately five orders of magnitude compared to the pure PMMA/PS. With an increase in the frequency of the applied field, the conductivity of charge carriers exhibits a linear rise, as these carriers can move more freely at high-frequency compared to low-frequency [47]. Furthermore, the dominance of the loss factor at high-frequency leads to a proportional enhancement in electrical conductivity within the high-frequencies range. Comparable patterns have been observed in various polymer nanocomposites [48, 49].

### 3.5 Dielectric Properties

The dielectric constant, represented by  $\epsilon'$ , is defined as the capacity of the material to store energy. In the presence of an electrical field, the dielectric loss ( $\epsilon''$ ), measures the extent of energy dissipation or loss within the medium [42]. In applications requiring high frequencies, lower dielectric constants provide enhanced insulation, thereby reducing the dissipation of energy as heat. High dielectric constant materials allow for the miniaturization of capacitors by enabling increased capacitance in a smaller footprint [49]. The following equations are used to calculate the values of  $\epsilon'$  and  $\epsilon''$ :

$$\epsilon' = \frac{Cd}{\epsilon_0 A} \quad (6)$$

$$\epsilon'' = \frac{\sigma}{\omega \epsilon_0} \quad (7)$$

Here,  $d$  stands for the film thickness,  $A$  denotes the cross-sectional area, and  $C$  represents the measured capacitance. Figure 8(A, B) depicts the variations in  $\epsilon'$  and  $\epsilon''$  across different frequencies in the investigated PMMA/PS-ZnO nanocomposites. With the increase in frequency, both  $\epsilon'$  and  $\epsilon''$  show a significant decline, reaching negligible levels. Additionally, it is believed that materials with polarity exhibit significant values of dielectric constant and dielectric loss at lower frequencies. However, as the frequency increases, these values decrease due to the inability of the dipoles to keep up with the changes in the field [50]. Following the incorporation of ZnO NPs, both  $\epsilon'$  and  $\epsilon''$  values experienced an increase across all frequency ranges. ZnO NPs exhibit characteristics akin to nanocapacitors when integrated into an insulating matrix [51]. The increasing concentration of ZnO nanoparticles creates localized electric fields. These fields can influence the orientation of polar molecules within the polymer matrix, causing them to align along the field direction [52]. The alignment of polar molecules due to the electric field from ZnO nanoparticles can enhance their mobility within the composite. This improved mobility likely contributes to the observed increase in the



**Fig. 8** Frequency dependence of dielectric properties in PMMA/PS-ZnO nanocomposites, (A) dielectric constant ( $\epsilon'$ ) and (B) dielectric loss ( $\epsilon''$ ) with  $\log(f)$  at room temperature

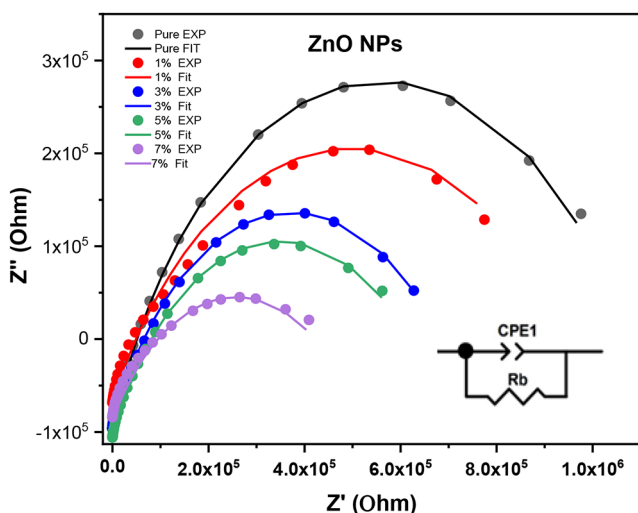
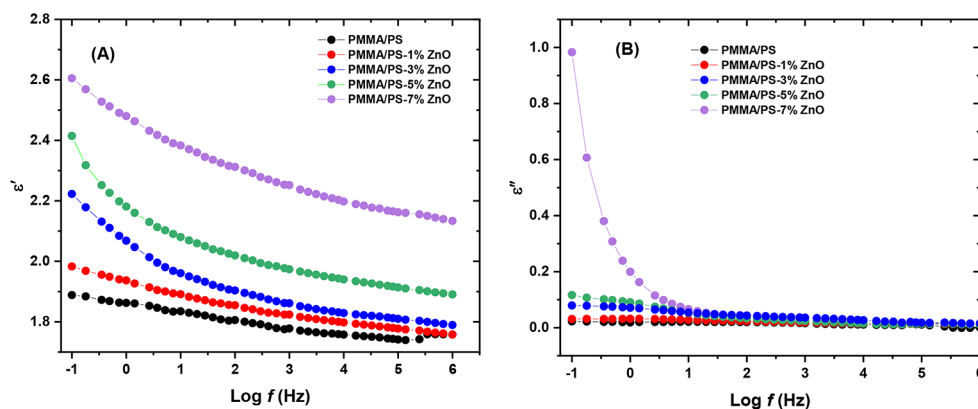


**Fig. 9** Nyquist plots for PMMA/PS doped with various ZnO NPs wt% and their equivalent circuit elements

dielectric constant. Nano-fillers are thought to enhance the dipole's dielectric constant by reducing constraints on its ability to react to electric fields [53, 54].

### 3.6 Complex Electric Modulus

The analysis of complex impedance data for the investigated samples can be facilitated through the application of the Eq. (8) [55]:

$$Z^* = Z' - iZ'' = \frac{1}{i\omega\epsilon_0\epsilon^*} \quad (8)$$

Here, the real and imaginary components of the complex impedance are represented by  $Z'$  and  $Z''$ , respectively. Fig. 9 illustrates the Nyquist curves for the prepared films. These curves were captured at room temperatures, spanning an extensive frequency range from 0.1 to 106 Hz. All Nyquist plots display a characteristic semi-circular arc positioned below the real axis ( $Z'$ ). This arc represents a parallel combination of bulk capacitance, originating from the stationary

polymeric matrix, and bulk resistance, resulting from the motion of ions [56]. The central depression in the semi-circular arc suggests a nonDebye ionic relaxation mechanism. The observed deviation from ideal Debye behavior could be attributed to a combination of factors, including surface roughness of the electrodes and potential variations in film thickness and morphology across the samples [57]. Moreover, with the increment in the concentrations of nanofillers, there is a reduction in the diameter of the semi-circle. This decrease indicates that the sample's ionic conductivity has increased and its bulk resistance has decreased. To elucidate the connection between the microstructure and electrical properties of the films, we present the impedance spectroscopy values interpreted through an equivalent circuit model comprised of resistors and capacitors. Fig. 9 (inset) presents the applied equivalent circuit representing the obtained impedance measurement. In this circuit, partial capacitance (CPE) and bulk resistance (Rb) are combined in parallel. The impedance of this CPE can be determined through the following [58]:

$$Z_{CPE} = 1/Q(i)^n \quad (9)$$

The correlation between the CPE parameter ( $n$ ) and the impedance magnitude ( $|Z|$ ) at  $\omega = 1$  rad/s (represented by  $Q$ ) reveals the deviation of the CPE from ideal capacitor behavior. A value of  $n = 1$  indicates a pure capacitor, while  $n = 0$  suggests a pure resistor. The equivalent circuit model parameters obtained by fitting the impedance data (Fig. 9) using the EIS program are presented in Table 3. As per the findings, the bulk resistance (Rb) decreases with the increase of nanofiller wt%, suggesting the presence of more interconnected conductive channels [59]. The decrease in Rb may be owing to the increase in charge carrier concentrations and the decline in crystallinity of the samples. Furthermore, the increase in ZnO NPs concentration corresponds to an elevation in bulk capacitance values ( $Q$ ), aligning with the previous description of the creation of numerous nanocapacitors

[60]. The modeling values align closely with the collected data, providing strong evidence for the appropriateness of the chosen equivalent circuit.

## 4 Conclusion

Zinc oxide nanoparticles (ZnO NPs) of varying wt% (1, 3, 5, and 7%) were introduced to polymer nanocomposite samples consisting of polymethyl methacrylate (PMMA) and polystyrene (PS) using the solution-casting method. The ZnO NPs were found to have a hexagonal structure with diameters ranging between 25 and 45 nm based on XRD and TEM investigations. According to XRD investigation, the produced samples' crystallinity decreases when ZnO NPs are incorporated into PMMA/PS. These nanocomposites' FT-IR spectra revealed that the inclusion of ZnO NPs resulted in a decrease in their vibrational peaks. The incorporation of additional ZnO nanoparticles led to significant changes in the optical band gap energies and UV-vis absorption spectra of the samples. There was a reduction in the bandgap energy ( $E_g$ ), transitioning from 4.45 eV to 3.12 eV for the direct bandgap and from 3.33 eV to 1.82 eV for the indirect bandgap. The AC conductivity ( $\sigma_{ac}$ ) of the nanocomposites displayed a marked increase with rising nanoparticle content. For instance, at a frequency of  $10^6$  Hz, the  $\sigma_{ac}$  value for the pure PMMA/PS blend was  $1.63 \times 10^{-17}$  S/cm, which significantly increased to  $3.14 \times 10^{-13}$  S/cm for the nanocomposite containing 7 wt% ZnO nanoparticles. The equivalent electrical circuits of the films were analyzed concerning their impedance components  $Z'$  and  $Z''$ . Both the decrease in sample crystallinity and the increasing concentration of charge carriers may be responsible for the bulk resistance decrease. Prepared nanocomposite samples have remarkable optical and electrical properties, rendering them ideal for use in flexible optoelectronic and capacitive energy storage systems.

**Author Contributions** Ghadah Abdulrahman AlZaidy: Investigation, Writing - Review & Editing.

**Funding** Not Applicable.

**Data Availability** The data that support the findings of this study are available on request from the corresponding author.

## Declarations

**Competing Interests** The authors declare that they have no known competing financial interests or personal relationships that could have appeared to influence the work reported in this paper.

## References

1. S.J. Almeahmadi et al., Improving the optical, photoluminescence, and electrical properties of PEO/NaAlg-WO<sub>3</sub> nanocomposites for optoelectronic and nanodielectric applications. *J. Mater. Res. Technol.* **26**, 2310–2318 (2023)
2. K.H. Alharbi et al., Optical, thermal, and electrical characterization of polyvinyl pyrrolidone/carboxymethyl cellulose blend scattered by tungsten-trioxide nanoparticles. *Polymers.* **15**(5), 1223 (2023)
3. D. Romero-Fierro et al., Polymer-magnetic semiconductor nanocomposites for industrial electronic applications. *Polymers.* **14**(12), 2467 (2022)
4. A.A. El-Gamal, *Optical and Electrical Properties of Polystyrene/Poly-methyl methacrylate Polymeric Blend Filled with Semiconductor and Insulator Nanofillers* physica status solidi –Rapid Research Letters, 2023. 17(10): p. 2300145
5. Z. Wang et al., Functional non-volatile memory devices: from fundamentals to photo-tunable properties. *Phys. Status solidi – Rapid Res. Lett.* **13**(5), 1800644 (2019)
6. L. Gaabour, Effect of addition of TiO<sub>2</sub> nanoparticles on structural and dielectric properties of polystyrene/polyvinyl chloride polymer blend. *AIP Adv.*, 2021. **11**(10)
7. A. Alsaad et al., Optical properties of transparent PMMA-PS/ZnO NPs polymeric nanocomposite films: UV-Shielding applications. *Mater. Res. Express.* **6**(12), 126446 (2020)
8. D. Mrđenović et al., Visualizing surface phase separation in PS-PMMA Polymer blends at the Nanoscale. *ACS Appl. Mater. Interfaces.* **14**(21), 24938–24945 (2022)
9. M. El-Morsy et al., Optical and electrical conductivity improvement of polystyrene/polymethyl methacrylate blend embedded by silver nanoparticles for electrical devices. *J. Mater. Sci.: Mater. Electron.* **34**(14), 1162 (2023)
10. H.M. Shanshool et al., Investigation of energy band gap in polymer/ZnO nanocomposites. *J. Mater. Sci.: Mater. Electron.* **27**, 9804–9811 (2016)
11. M.A. Kadhim, E. Al-Bermamy, New fabricated PMMA-PVA/graphene oxide nanocomposites: structure, optical properties and application. *J. Compos. Mater.* **55**(20), 2793–2806 (2021)
12. A.M. Kadim et al., Effect of Loading Corn Starch nanoparticles on the Morphological, Optical, and Dielectric behaviors of PVA/PMMA/PAAm polymer blend for optoelectronic and antibacterial applications. *Nano Biomed. Eng.*, 2024. **16**(1)
13. K.J.S. Abdali, *Novel flexible glass composite film for stretchable devices applications* 2023. 15(12): pp. 5187–5195
14. G. Soni et al., Optical, mechanical and structural properties of PMMA/SiO<sub>2</sub> nanocomposite thin films. *Mater. Res. Express.* **5**(1), 015302 (2018)
15. Q. Al-Bataineh et al., *Optical characterizations of PMMA/metal oxide nanoparticles thin films: bandgap engineering using a novel derived model.* *Heliyon* **7**: e05952. 2021
16. N. Cinausero et al., Impact of modified alumina oxides on the fire properties of PMMA and PS nanocomposites. *Polym. Adv. Technol.* **22**(12), 1931–1939 (2011)
17. J. Wie, J. Kim, Thermal conductivity enhancement derived from poly (methyl methacrylate)-grafted carbon nanotubes in poly (methyl methacrylate)/polystyrene blends. *Polymers.* **11**(8), 1347 (2019)
18. E.H. Alsharaeh, Polystyrene-poly (methyl methacrylate) silver nanocomposites: significant modification of the thermal and electrical properties by microwave irradiation. *Materials.* **9**(6), 458 (2016)
19. S.S. Ali et al., MWCNTs/PMMA/PS composites functionalized PANI: electrical characterization and sensing performance for

- ammonia detection in a humid environment. *Sens. Actuators B: Chem.* **320**, 128364 (2020)
20. R. Mathur et al., Electrical and mechanical properties of multi-walled carbon nanotubes reinforced PMMA and PS composites. *Polym. Compos.* **29**(7), 717–727 (2008)
  21. F.L. Rashid et al., Preparation of (PS-PMMA) copolymer and study the effect of Sodium Fluoride on its optical properties. 2013. **4**(2): p. 121–126
  22. E. Abdelrazek et al., Physical properties of MnCl<sub>2</sub> fillers incorporated into a PVDF/PVC blend and their complexes. 2009. **15**(3): p. 171–177
  23. T. Khalafi, F. Buazar, K. Ghanemi, Phycosynthesis and enhanced photocatalytic activity of zinc oxide nanoparticles toward organosulfur pollutants. *Sci. Rep.* **9**(1), 6866 (2019)
  24. T.I. Al-Naggar, B. El-Badry, Structural, optical and electrical properties of poly (Methyl Methacrylate) polymer under alpha radiation. *Nuclear Instruments Methods Phys. Res. Sect. B: Beam Interact. Mater. Atoms.* **508**, 24–28 (2021)
  25. H. Ragab et al., Incorporating hybrid Ag/Co<sub>2</sub>O<sub>3</sub> nanofillers into PVP/CS blends for multifunctional optoelectronic and nanodielectric applications. *Ceram. Int.* **50**(1), 1254–1262 (2024)
  26. O.G. Abdullah et al., Characterization of polyvinyl alcohol film doped with sodium molybdate as solid polymer electrolytes. *J. Mater. Sci.: Mater. Electron.* **28**, 8928–8936 (2017)
  27. A. Rajeh, H. Ragab, M.M. Abutalib, Co doped ZnO reinforced PEMA/PMMA composite: structural, thermal, dielectric and electrical properties for electrochemical applications. *J. Mol. Struct.* **1217**, 128447 (2020)
  28. A. Tarabiah et al., Enhanced structural, optical, electrical properties and antibacterial activity of PEO/CMC doped ZnO nanorods for energy storage and food packaging applications. *J. Polym. Res.* **29**(5), 167 (2022)
  29. E. Fekete, B. Pukánszky, Effect of molecular interactions on the miscibility and structure of polymer blends. *Eur. Polymer J.* **41**(4), 727–736 (2005)
  30. H. Ragab, Improved physical, thermal, and conductivity strength of ternary nanocomposite films of PVDF/PMMA/GO NPs for electrical applications. *J. Polym. Res.* **29**(6), 219 (2022)
  31. M. El-Morsy et al., Optical and electrical conductivity improvement of polystyrene/polymethyl methacrylate blend embedded by silver nanoparticles for electrical devices. 2023. **34**(14): p. 1162
  32. L.M. Cardoso et al., New polymorphic phase of arachidic acid crystal: structure, intermolecular interactions, low-temperature stability and Raman spectroscopy combined with DFT calculations. *RSC Adv.* **13**(48), 34032–34044 (2023)
  33. B.K. Sharma et al., Dielectric properties of nano ZnO-polyaniline composite in the microwave frequency range. *J. Alloys Compd.* **477**(1–2), 370–373 (2009)
  34. R. Sengwa, N. Kumar, M. Saraswat, Morphological, structural, optical, broadband frequency range dielectric and electrical properties of PVDF/PMMA/BaTiO<sub>3</sub> nanocomposites for futuristic microelectronic and optoelectronic technologies. *Mater. Today Commun.* **35**, 105625 (2023)
  35. S. Suvarna, M. Ramesan, Optical and electrical properties of copper alumina nanoparticles reinforced chlorinated polyethylene composites for optoelectronic devices. *J. Indian Chem. Soc.* **99**(11), 100772 (2022)
  36. K. Meera, M.T. Ramesan, Development of high-performance biopolymer nanocomposites derived from carboxymethyl chitosan/boehmite via green synthesis. *Polym. Compos.* **44**(2), 1135–1148 (2023)
  37. A.N. Al-hakimi et al., Inorganic nanofillers TiO<sub>2</sub> nanoparticles reinforced host polymer polypyrrole for microelectronic devices and high-density energy storage systems. *J. Mater. Sci.: Mater. Electron.* **34**(3), 238 (2023)
  38. M. Farea, A. Abdelghany, A.J.R. Oraby, Opt. Dielectric Characteristics Polyethyl. oxide/sodium alginate-modified gold. *Nanocomposites.* **10**(62), 37621–37630 (2020)
  39. K. Parvathi, M.T. Ramesan, Effect of titanium dioxide on the structural, thermal, and electrical properties of chlorinated natural rubber/poly (indole) blend nanocomposites for flexible nanoelectronic devices. *J. Appl. Polym. Sci.* **140**(11), e53621 (2023)
  40. A. Al-Ojeery, M. Farea, Optical and dielectric properties of polymer nanocomposite based on PEG/NaAlg blend and Ag/Au nanoparticles prepared by green synthesis method for energy storage applications. *Opt. Quantum Electron.* **55**(11), 988 (2023)
  41. R.A. Pashameah et al., Modification and development of the optical, structural, thermal and electrical characterization of Chitosan incorporated with Au/Bi<sub>2</sub>O<sub>3</sub>/Mo NPs fabricated by laser ablation. *J. Inorg. Organomet. Polym. Mater.* **32**(7), 2729–2736 (2022)
  42. H. Ragab, M. Farea, *Structural, optical, and electrical enhancement of polyethylene oxide (PEO) and sodium alginate (NaAlg) through embedding silver nanoparticles (Ag NP) for optoelectrical applications* *Journal of Materials Science: Materials in Electronics*, 2023. **34**(31): p. 2079
  43. E. Salim, A. Tarabiah, The influence of NiO nanoparticles on Structural, Optical and Dielectric properties of CMC/PVA/PEDOT: PSS nanocomposites. *J. Inorg. Organomet. Polym. Mater.*, 2023: p. 1–8
  44. M. Morsi et al., Hybrid MWCNTs/Ag nanofiller reinforced PVP/CMC blend-based polymer nanocomposites for multifunctional optoelectronic and nanodielectric applications. 2023. **31**(2): p. 664–676
  45. A. Waly, A. Abdelghany, A. Tarabiah, Study the structure of selenium modified polyethylene oxide/polyvinyl alcohol (PEO/PVA) polymer blend. *J. Mater. Res. Technol.* **14**, 2962–2969 (2021)
  46. H.A. Alsalmah et al., Hybrid GO/TiO<sub>2</sub> nanoparticles reinforced NaAlg/PVA blend: nanocomposites for high-performance energy storage devices. *Polym. Adv. Technol.* **34**(9), 2831–2840 (2023)
  47. K. Hemalatha et al., Temperature dependent dielectric and conductivity studies of polyvinyl alcohol-ZnO nanocomposite films by impedance spectroscopy. *J. Appl. Phys.*, 2015. 118(15).
  48. M. Yang et al., Largely enhanced dielectric constant of PVDF nanocomposites through a core-shell strategy. *Phys. Chem. Chem. Phys.* **20**(4), 2777–2786 (2018)
  49. H. Ragab et al., Effect of CsBr on the optical properties and electrical conductivity of PVP/PVA composite for flexible optoelectronic devices. *Inorg. Chem. Commun.* **159**, 111741 (2024)
  50. E.M. Abdelrazek et al., Mechanical and electrical studies of PVA/PVP blend filled with MWCNTs. *Polym. Bull.* **80**(6), 6693–6706 (2023)
  51. A. Menazea et al., Facile synthesis and high-performance dielectric properties of polyethylene oxide-chitosan-iron oxide nanocomposite for electrical applications. *J. Mater. Res. Technol.* **18**, 2273–2281 (2022)
  52. El H.G. Gohary et al., Studies of the Structural, Optical, Thermal, Electrical and Dielectric properties of a Polyvinyl Alcohol/Sodium Alginate Blend Doped with Cu nanoparticles and ZnO Nanorods as Hybrid Nanofillers for Use in Energy Storage devices. *J. Polym. Environ.*, 2023: p. 1–11
  53. Y. Thakur et al., Enhancement of the dielectric response in polymer nanocomposites with low dielectric constant fillers. *Nanoscale.* **9**(31), 10992–10997 (2017)
  54. A. Menazea et al., Enhanced dielectric properties of  $\alpha$ -MoO<sub>3</sub> nanobelts dispersed polyethylene oxide-carboxymethyl cellulose matrix-based nanocomposites. 2024. **312**: p. 128585
  55. R. Khalil, Impedance and modulus spectroscopy of poly (vinyl alcohol)-Mg [ClO<sub>4</sub>]<sub>2</sub> salt hybrid films. *Appl. Phys. A* **123**(6), 422 (2017)

56. A. Al-Muntaser et al., Incorporated TiO<sub>2</sub> nanoparticles into PVC/PMMA Polymer blend for enhancing the optical and electrical/dielectric properties: hybrid nanocomposite films for flexible optoelectronic devices. *Polym. Eng. Sci.* **63**(11), 3684–3697 (2023)
57. S. Lanfredi et al., Electric conductivity and relaxation in fluoride, fluorophosphate and phosphate glasses: analysis by impedance spectroscopy. *Solid State Ionics.* **146**(3–4), 329–339 (2002)
58. A. Al-Muntaser et al., Tuning the structural, optical, electrical, and dielectric properties of PVA/PVP/CMC ternary polymer blend using ZnO nanoparticles for nanodielectric and optoelectronic devices. *Opt. Mater.* **140**, 113901 (2023)
59. D.A. Nasrallah, E.G. El-Metwally, A.M. Ismail, Structural, thermal, and dielectric properties of porous PVDF/Li<sub>4</sub>Ti<sub>5</sub>O<sub>12</sub> nanocomposite membranes for high-power lithium-polymer batteries. *Polym. Adv. Technol.* **32**(3), 1214–1229 (2021)
60. M. Rahaman et al., High density polyethylene and metal oxides based nanocomposites for high voltage cable application (2021)

**Publisher's Note** Springer Nature remains neutral with regard to jurisdictional claims in published maps and institutional affiliations.

Springer Nature or its licensor (e.g. a society or other partner) holds exclusive rights to this article under a publishing agreement with the author(s) or other rightsholder(s); author self-archiving of the accepted manuscript version of this article is solely governed by the terms of such publishing agreement and applicable law.